

# Two-Dimensional Intensity Distribution and Adaptive Power Allocation for Ultraviolet Ad-Hoc Network

Hong Qi, Difan Zou, Chen Gong<sup>✉</sup>, *Senior Member, IEEE*, and Zhengyuan Xu<sup>✉</sup>, *Senior Member, IEEE*

**Abstract**—We consider a directional antenna array in an ultraviolet (UV) scattering communication ad-hoc network. To efficiently characterize the link gain coverage of a single antenna, we propose an algorithm based on one-dimensional (1D) numerical integration and an off-line data library. We also investigate the two-dimensional (2D) scattering intensity distribution, which shows that the link gain profile can be well fitted by elliptic models. In addition, assuming that the node distribution of an ad-hoc network obeys Poisson point process (PPP), we investigate the network connectivity probability and the minimum power that the network remains connected under different antenna parameters, and compare the performance of directional antenna array with that of omnidirectional antenna array. Numerical results show that employing directional antenna arrays can effectively reduce the power required for network connectivity. Moreover, we consider a two-layer network using directional antenna array, and design adaptive node assignment and power allocation to increase the minimum rate. Numerical results show that the proposed algorithm can improve the minimum node rate by more than 10%. Moreover, similar performance gain can be observed even considering the overhead of a media-access control (MAC) layer protocol.

**Index Terms**—Ultraviolet wireless scattering communication, ad-hoc network, directional antenna array.

## I. INTRODUCTION

OPTICAL wireless communication serves as an alternative transmission solution when the radio-frequency (RF) is prohibited. An important requirement of optical wireless communication is the alignment of transmitter and receiver, but this requirement is an important constraint on the real application scenario. Non-line-of-sight (NLOS) ultraviolet (UV) communication alleviates the requirements on line-of-sight (LOS)

Manuscript received April 7, 2021; revised June 14, 2021 and July 23, 2021; accepted July 29, 2021. Date of publication August 3, 2021; date of current version February 16, 2022. This work was supported in part by the National Key Research and Development Program of China under Grant 2018YFB1801904; in part by the Key Program of National Natural Science Foundation of China under Grant 61631018; and in part by the Key Research Program of Frontier Sciences of CAS under Grant QYZDY-SSW-JSC003. This article was presented in part at ICC 2020, Dublin, Ireland, Jul. 2020. The editor coordinating the review of this article was H. Tabassum. (*Corresponding author: Chen Gong.*)

Hong Qi, Chen Gong, and Zhengyuan Xu are with the Key Laboratory of Wireless-Optical Communications, Chinese Academy of Sciences, University of Science and Technology of China, Hefei 230027, Anhui, China (e-mail: hongqi@mail.ustc.edu.cn; cgong821@mail.ustc.edu.cn; xuzy@mail.ustc.edu.cn).

Difan Zou is with the University of California at Los Angles, Los Angles, CA 90095 USA (e-mail: knowzou@mail.ustc.edu.cn).

Digital Object Identifier 10.1109/TGCN.2021.3102062

links, and thus can support user mobility, which can be adopted as an important supplement. Due to extremely weak solar background radiation, the scattering characteristics of UV light can guarantee NLOS link [1]–[4].

Recently, NLOS UV scattering communication are widely investigated for point to point (p2p) scenario, based on which the channel modeling [5], [6], signal characterization and performance analysis [7]–[9] are studied from both the transmitter and receiver sides. The connectivity performance for an UV ad-hoc network has been studied in [10], [11]. Note that the existing works basically focus on single-link analysis and network connectivity. The detailed shape of the coverage area and the relationship with the UV source parameters have not been characterized. In [12], Monte Carlo method is adopted to simulate the influence of different transceiver parameters on the path loss. However, for the receiver end with a fixed structure, the coverage characteristics of the transmitter not only facilitate the deployment of nodes in the network, but also provide a concise representation on the link gain between communication nodes. In addition, the transmitter configuration also determines the effective communication range of the node, but how it affects the performance of typical ad-hoc network has not been analyzed. The above two fundamental characteristics are crucial for the analysis and design of UV communication network.

Traditionally, the UV scattering communication link gain can be obtained based on Monte Carlo method [3], [13], theoretical analysis [14]–[17] and experimental results [18], [19]. In [14], [16], the analytical method is more effective for link calculation with small receiving field-of-view (FOV). In [15], triple integration is adopted with high computational complexity. Therefore, for low complexity requirements, analytical or semi-analytical methods need to be explored to obtain the intensity distribution.

On the other hand, UV scattering communication is typically applied to a temporary communication network, typically in the form of an ad-hoc network [20]. In [21], ultraviolet scattering communication is applied to the sensor ad-hoc network, and the influence of the FOV of the scattering antenna on the received power is analyzed. In [11], the connectivity problem in the ultraviolet scattering network is investigated, in particular the influence of node density and transmission power on the  $k$ -connectivity of the network. In [22], the expression of isolation probability in multi-hop ultraviolet scattering network is given. Current works focus

on analyzing the basic indicators of the ad-hoc network, but the network structure is relatively simple, and the influence of the antenna structure on the network performance is not involved.

In this work, a two-layer communication network can be considered, where mobile communication vehicles are used as the first-layer nodes and randomly distributed user terminals as the second-layer nodes. Moreover, since the nodes are randomly distributed, power control of the first-layer nodes is essential to improve node performance and reduce interference, which needs to be delicately designed.

The contributions of our work are summarized as follows.

- We consider a laser source, and propose an analytical approximation to the link gain as a function of the elevation angle and the receiver's two-dimensional (2D) position. Based on the proposed algorithm, the 2D scattering intensity distribution pattern is discussed. It is observed that the elliptical model can well fit the contour.
- We characterize the shape parameters based on the source elevation angle and divergence angle, and give the contour line fitting expression when the path loss is fixed at different elevation angles.
- In the ad-hoc network, the influence of the directional antenna array and the omnidirectional antenna on the network performance is compared, and the recommended value of the optimal antenna structure design parameter is given.
- We consider a typical two-layer ad-hoc network, and propose iterative node allocation and power control algorithms. We investigate the performance of the proposed algorithms under the overhead of a media-access control (MAC) layer protocol, as well as the robustness of the proposed algorithm. It is seen that the proposed node allocation and power control algorithms outperform various comparison benchmarks.

The remainder of this paper is organized as follows. In Section II, we provide a method to efficiently represent the link gain of scattering communication, and investigate the coverage pattern of the directional antenna array. In Section III, we analyze the performance of the directional antenna array and a single omnidirectional antenna, and give the influence of antenna parameters on performance. In Section IV, we consider a two-layer network, propose an adaptive node assignment and power allocation approach to optimize the minimum user capacity under sum capacity and node connectivity constraints, and investigate the performance of the proposed network structure assuming overhead of a MAC layer protocol. Finally, Section V concludes this paper.

## II. TWO-DIMENSIONAL INTENSITY DISTRIBUTION OF SCATTERING

### A. Scattering Model With Efficient Link Gain Representation

Consider the atmospheric UV communication with both scattering and absorption. In general, Rayleigh scattering coefficient  $k_s^{ray}$ , Mie scattering coefficient  $k_s^{mie}$ , and absorption coefficient  $k_a$  are adopted to characterize the scattering and absorption intensities. Moreover, let  $k_s = k_s^{ray} + k_s^{mie}$  and

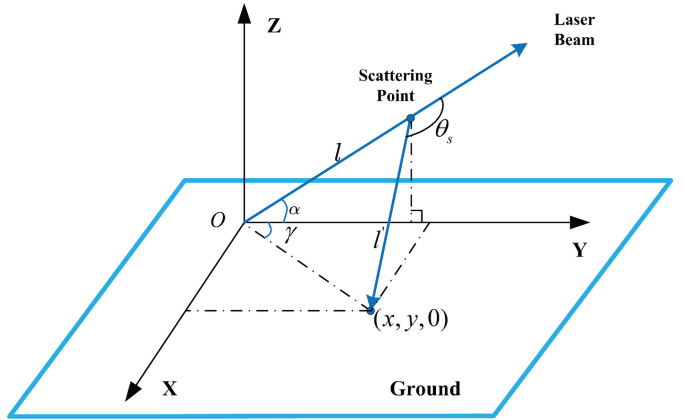


Fig. 1. The geometric description of UV scattering radiation.

$k_t = k_a + k_s$  denote the scattering coefficient and total extinction coefficient, respectively.

In order to specify the achievable communication area, it is necessary to analyze the contour of such 2D intensity distribution to obtain an approximate achievable communication area for different user positions. The geometric configuration of the transmission path is shown in Figure 1. The transmitter position is set to be  $(0, 0, 0)$ . Let  $(x, y, 0)$  denote the receiver position,  $l$  and  $l'$  denote the distances from scattering point to the transmitter and receiver, respectively. Let  $\alpha$  be the elevation angle between the light direction and  $Y$ -axis,  $\theta_s$  be the scattering angle between the light direction and the line from scattering point to the receiver,  $\Omega(l)$  be the solid angle of Rx at each scattering point  $(0, l \cos \alpha, l \sin \alpha)$ , and  $A_r$  be the area of receiver aperture.

Letting  $E_t$  be the intensity of transmitted UV signal, the power of signal scattered at  $(0, l \cos \alpha, l \sin \alpha)$  and detected by the receiver is given by

$$dE_r(l) = E_t P[\mu(l)] \Omega(l) e^{-k_a(l+l')} e^{-k_s l'} \delta l, \quad (1)$$

where  $\mu(l) = \cos \theta_s$  is a function of  $x, y, \alpha$ , and  $l$ , given by  $\mu(x, y, \alpha, l) = \frac{y \cos \alpha - l}{l'}$ ; and  $\Omega(l)$  denotes the solid angle from receiving area to scattering point  $(0, l \cos \alpha, l \sin \alpha)$ , given by  $\Omega(x, y, \alpha, l) = \frac{A_r}{l'^2} \frac{l \sin \alpha}{l'}$ .

Let  $P(\mu)$  denote the scattering phase function. Considering the dominant Rayleigh scattering and Mie scattering, it can be determined by the corresponding scattering phase functions given by [3],

$$P(\mu) = \frac{k_s^{Ray}}{k_s} p^{Ray}(\mu) + \frac{k_s^{Mie}}{k_s} p^{Mie}(\mu), \quad (2)$$

where  $k_s^{Ray} = 2.66 \times 10^{-4}/m$  and  $k_s^{Mie} = 2.84 \times 10^{-4}/m$  represent Rayleigh and Mie scattering coefficients, respectively; Rayleigh and Mie scattering phase functions are given by

$$\begin{aligned} p^{Ray}(\mu) &= \frac{3[1 + 3\gamma + (1\gamma)\mu^2]}{16\pi(1+2\gamma)}, \\ p^{Mie}(\mu) &= \frac{1-g^2}{4\pi} \left\{ \frac{1}{(1+g^2-2g\mu)^3/2} \right\} + f \frac{3\mu^2 - 1}{2(1+g^2)^3/2}, \end{aligned} \quad (3)$$

where  $\gamma, f, g$  represent scattering model parameters merely related to the communication environment, with typical values  $\gamma = 0.017, f = 0.5$  and  $g = 0.2$  [23].

In the atmosphere, free distance  $l$  satisfies exponential distribution  $f(l) = k_s e^{-k_s l}$ . Then, the total received power at  $(x, y, 0)$  is given by

$$E_r = \int_0^\infty E_t P[\mu(l)] \Omega(l) k_s e^{-(k_a+k_s)(l+l')} dl. \quad (4)$$

Hence, link gain function  $L_g(x, y, \alpha)$  is given by

$$L_g(x, y, \alpha) = \int_0^\infty P(\mu) \Omega(l) k_s e^{-(k_a+k_s)(l+l')} dl. \quad (5)$$

The one-dimensional (1D) numerical integration can reduce the simulation time dramatically compared with Monte Carlo method [3], [13]. However, it still requires high computational complexity. To address this issue, we investigate whether it can be represented by variables in a lower-dimensional space. Motivated by this, we provide the following result.

*Theorem 1:* If the link gain is calculated in accordance with (5), we have the following,

$$L_g(x, y, \alpha) = \frac{L_g(0, \sqrt{x^2 + y^2}, \alpha') \sin \alpha}{\sin \alpha'}, \quad (6)$$

where  $\cos \alpha' = \frac{y}{y'} \cos \alpha = \cos \alpha \cos \gamma$  represents the cosine of elevation angle after projection, and  $\tan \gamma = \frac{x}{y}$ .

*Proof:* For the link gain  $L_g(x, y, \alpha)$ , we have

$$\begin{aligned} l'^2 &= x^2 + (y - l \cos \alpha)^2 + l^2 \sin^2 \alpha \\ &= y'^2 + l^2 - 2y'l \cos \alpha', \end{aligned} \quad (7)$$

where  $y' = \sqrt{x^2 + y^2}$ . This equation implies that  $l'(x, y, \alpha, l) = l'(0, y', \alpha', l)$ . For the cosine of scattering angle, we have

$$\mu(x, y, \alpha, l) = \cos \theta_s = \frac{y \cos \alpha - l}{l'} = \frac{y' \cos \alpha' - l}{l'}, \quad (8)$$

which implies that  $\mu(x, y, \alpha, l) = \mu(0, y', \alpha', l)$ . For solid angle  $\Omega(x, y, \alpha, l)$ , we have

$$\begin{aligned} \Omega(x, y, \alpha, l) &= \frac{A_r l \sin \alpha'}{l^3} \frac{\sin \alpha}{\sin \alpha'} \\ &= \Omega(0, y', \alpha', l) \frac{\sin \alpha}{\sin \alpha'}. \end{aligned} \quad (9)$$

Substituting the above results into equation (5), we have

$$\begin{aligned} L_g(x, y, \alpha) &= \int_0^\infty P(\mu) \Omega(x, y, \alpha, l) k_s e^{-(k_a+k_s)(l+l')} dl \\ &= \int_0^\infty P(\mu') \Omega(0, y', \alpha', l) \frac{\sin \alpha}{\sin \alpha'} k_s \\ &\quad \times e^{-(k_a+k_s)(l+l')} dl \\ &= L_g(0, y', \alpha') \frac{\sin \alpha}{\sin \alpha'}, \end{aligned} \quad (10)$$

where  $\mu' \triangleq \mu(0, y', \alpha', l)$ . ■

Based on the above arguments, a 2D library  $\mathbf{L} \triangleq \{L(0, r_i, \alpha_i), r_i \in \mathbf{r}, \alpha_i \in \boldsymbol{\alpha}\}$  is constructed, where  $\mathbf{r}$  denotes the set of different communication ranges when the receiver locates at  $Y$ -axis, and  $\boldsymbol{\alpha}$  denotes the set of different elevation angles (typically we set  $\mathbf{r} = [0 : 1 : 1000]$  and

$\boldsymbol{\alpha} = \pi \times [0.005 : 0.005 : 1]$ ). Then, link gain  $L_g(x, y, \alpha)$  can be calculated by obtaining  $L_g(0, (x^2 + y^2)^{1/2}, \alpha')$  from library  $\mathbf{L}$ , and multiplying by  $\sin \alpha / \sin \alpha'$ , where  $\tan \alpha' = x/y$ . For a special case that  $\alpha = 90^\circ$ , we have  $\alpha' = 90^\circ$  and  $L_g(x, y, 90^\circ) = L_g(0, \sqrt{(x^2 + y^2)}, 90^\circ)$ , which implies a circular shape for the contour of 2D scattering intensity distribution.

Assume uniform pattern for the beam produced by the light source. In order to calculate the link gain for a wide-beam source, we generate multiple narrow beams with uniformly distributed random direction, and average the corresponding link gains. Assume the center direction of light is  $(0, \cos \alpha, \sin \alpha)$ , and the full divergence angle is  $\phi_d$ . Let  $\zeta' = (\zeta'_x, \zeta'_y, \zeta'_z)$  denote the random emitting direction. It can be generated according to the coordinate transformation, specified by

$$\begin{aligned} \zeta'_x &= \sin \theta_s' \sin \phi', \\ \zeta'_y &= -\sin \theta_s' \cos \phi' \sin \alpha + \cos \theta_s' \cos \alpha, \\ \zeta'_z &= \sin \theta_s' \cos \phi' \cos \alpha + \cos \theta_s' \sin \alpha, \end{aligned} \quad (11)$$

where  $\theta_s'$  and  $\phi'$  are random angles generated by  $\theta_s' = \arccos[1 - \tau(1 - \cos \frac{\phi_d}{2})]$  and  $\phi' = 2\pi\tau$ , where  $\tau$  denotes a uniformly distributed random variable between zero and one.

Let  $L'_g(x, y, \zeta')$  denote the link gain for the laser with normalized direction  $\zeta'$ , which can be mapped into standard form  $L_g(x', y', \alpha')$  via coordinate transformation, given by

$$\begin{aligned} x' &= \frac{\zeta'_y}{\sqrt{1 - \zeta_z'^2}} x - \frac{\zeta'_x}{\sqrt{1 - \zeta_z'^2}} y, \\ y' &= \frac{\zeta'_x}{\sqrt{1 - \zeta_z'^2}} x + \frac{\zeta'_y}{\sqrt{1 - \zeta_z'^2}} y. \end{aligned} \quad (12)$$

Hence, for each laser beam, we can obtain the corresponding link gain based on library  $\mathbf{L}$ . By averaging the link gains of sufficiently large number  $K$  of randomly generated narrow beams, we have the following link gain with a wide-beam source,

$$L_g^{WB}(x, y, \alpha, \phi_d) = \frac{1}{K} \sum_{k=1}^K L'_g(x, y, \zeta'_k), \quad (13)$$

where  $\zeta'_k$  denotes the random sending direction of the photon in the  $k$ -th simulation realization.

### B. Coverage With Different Elevation Angles

Assuming that the receivers are distributed in a squared area, we obtain a 2D scattering intensity distribution according to the above formulas. Specifically, we simulate  $500 \times 500$  link gains in area  $[-500, 500]m \times [-500, 500]m$ , and the 2D radiation distribution for the laser source with elevation angle  $\alpha = 30^\circ$  is shown in Figure 2(a).

In order to verify the accuracy of the proposed method, Monte Carlo method is used to calculate the path loss of each point under the same simulation parameters [3], [13]. The simulation results are demonstrated as shown in Figure 2(b).

It can be seen that the path loss distribution is basically the same as those of the proposed method, but the proposed

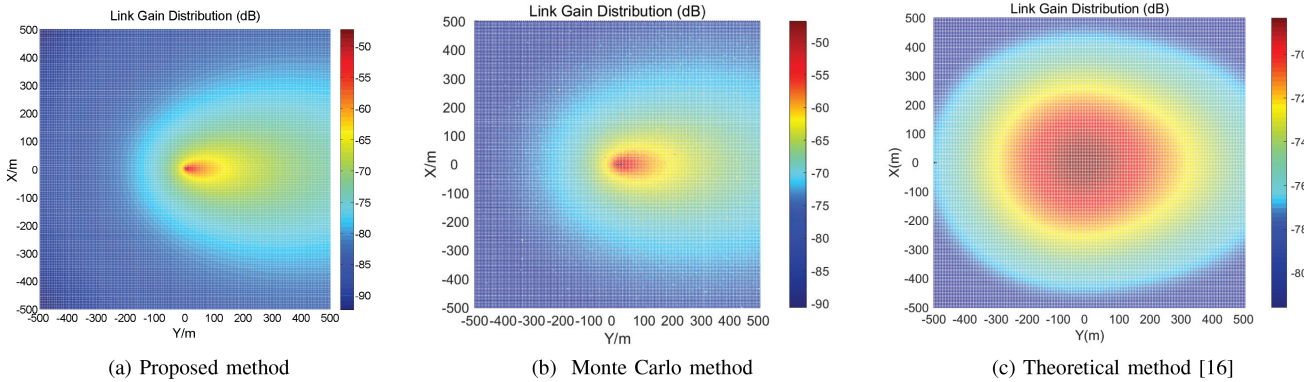


Fig. 2. The 2D radiation distribution for laser source with elevation angle  $\alpha = 30^\circ$ .

method has lower complexity, where the simulation time of Figure 2(b) is about 1000 times as that of Figure 2(a). Comparing the link gain results of the two methods, it can be found that the average path gain of the proposed method is  $1.1396\text{dB}$  higher than that of Monte Carlo method, and the standard deviation is  $1.4755\text{dB}$ .

We also compared the proposed approach with the typical theoretical method [16]. Under the same atmospheric parameters, the link gain results are demonstrated as shown in Figure 2(c). Significantly different link gain contours can be observed. It can be found that the average path gain of the method in reference [16] is  $3.1163\text{dB}$  lower than that of the Monte Carlo method, and the standard deviation is  $2.8966\text{dB}$ . It is seen that compared with the approach in reference [16], the proposed method shows closer mean path gain and lower standard deviation from the Monte Carlo approach.

It can be observed that the contour can be fitted by an ellipse. Motivated by this, we extract the contour coordinates, denoted as  $(\mathbf{X}, \mathbf{Y}) = \{(x_i, y_i), i = 1, 2, \dots, R\}$ . Then, we perform fitting based on the following elliptic function

$$\frac{(x - x_0)^2}{a^2} + \frac{(y - y_0)^2}{b^2} = 1, \quad (14)$$

where  $x_0 = 0$  due to the fact  $L_g(x, y, \alpha) = L_g(-x, y, \alpha)$ . The ellipse parameters  $(y_0, a, b)$  can be obtained based on the following least squares criterion

$$\min_{y_0, a, b} \sum_{i=1}^R \left[ a^2 \left( 1 - \frac{y_0^2}{b^2} + \frac{2y_0}{b^2} y_i - \frac{y_i^2}{b^2} \right) - x_i^2 \right]^2. \quad (15)$$

Letting  $\mathbf{k} = [a(1 - \frac{y_0^2}{b^2}), \frac{2a^2 y_0}{b^2}, -\frac{a^2}{b^2}]^T$  denote the parameter vector, the optimal fitting solution is given by

$$\mathbf{k} = \left( \mathbf{Y}_{R,3}^T \mathbf{Y}_{R,3} \right)^{-1} \mathbf{Y}_{R,3}^T \mathbf{x}_2, \quad (16)$$

where  $\mathbf{Y}_{R,3}$  is a 3-order Vandermonde matrix of parameters  $\{y_1, y_2, \dots, y_R\}$  and  $\mathbf{x}_2 \triangleq [x_1^2, x_2^2, \dots, x_R^2]^T$ .

Figure 3 shows the contours and the corresponding fitting ellipses for elevation angle from  $10^\circ$  to  $90^\circ$ , where the link threshold is set to be  $10^{-7}$ . It can be seen that the ellipse curve can well model the contour of 2D radiation distribution. As the elevation angle increases, the coverage area decreases, and the contour becomes a circle when  $\alpha = 90^\circ$ .

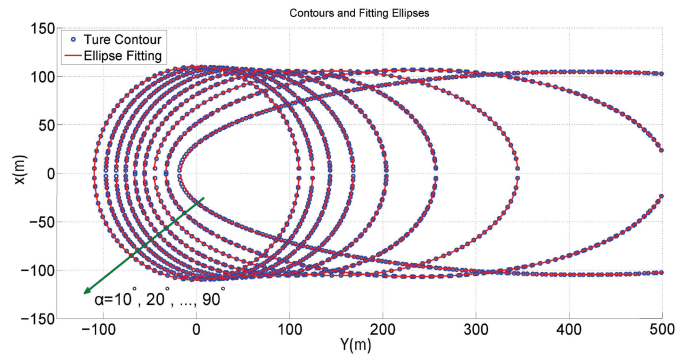


Fig. 3. The contours and fitting ellipses of 2D radiation distribution for the laser source with elevation angle from  $10^\circ$  to  $90^\circ$  ( $L_g = 10^{-7}$ ).

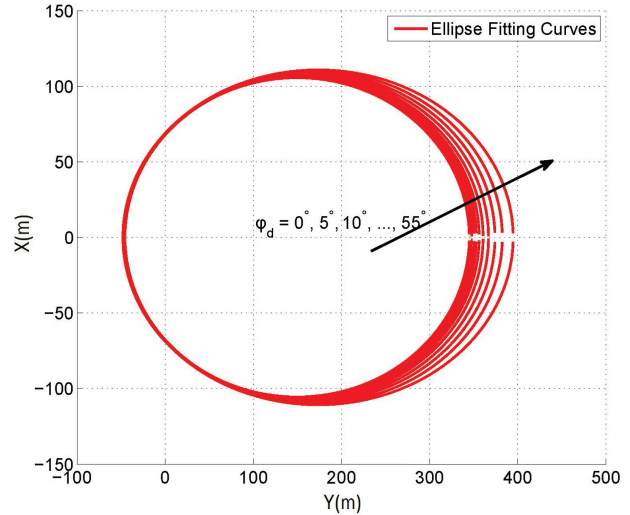


Fig. 4. The ellipse fitting of the contour of 2D radiation distribution for  $(\alpha, \phi_d) = (30^\circ, 0^\circ - 55^\circ)$  ( $L_g = 10^{-7}$ ).

### C. Coverage for Different Divergence Angles

We investigate the relationship between the ellipse characteristics and divergence angle  $\phi_d$ . Figure 4 shows that the contour size increases with respect to the divergence angle, but not sensitive to it. Moreover, it can be observed that the left endpoint of the fitting ellipses basically remains the same but the right endpoint only changes from  $(0, 350)$  to  $(0, 400)$ .

TABLE I  
FIT OF TRANSMISSION AND ELLIPSE PARAMETERS

$\alpha$	$1/L_g$	$y_1(m)$	$a(m)$
10°	$6.7b^2 + 954.9b + 6801$	$0.987b + 0.950$	$b \sin 10^\circ$
20°	$19.3b^2 + 2058b + 20780$	$0.879b + 2.980$	$b \sin 20^\circ$
30°	$36.9b^2 + 2882b + 45220$	$0.735b + 4.774$	$b \sin 30^\circ$
40°	$58.4b^2 + 2995b + 89750$	$0.583b + 5.973$	$b \sin 40^\circ$
50°	$182.19b^2 + 2052b + 167900$	$0.439b + 6.421$	$b \sin 50^\circ$
60°	$106.7b^2 - 119.2b + 293200$	$0.310b + 6.001$	$b \sin 60^\circ$
70°	$130.2b^2 - 3577b + 481600$	$0.196b + 4.799$	$b \sin 70^\circ$
80°	$1151.3b^2 - 8182b + 744400$	$0.094b + 2.784$	$b \sin 80^\circ$
90°	$168.4b^2 - 13750b + 1096000$	0	$b$

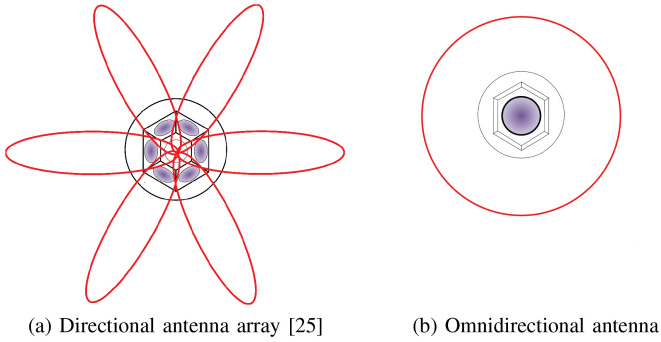


Fig. 5. The coverage of different transmitter antenna structures.

To characterize the link coverage in the ad-hoc network, we fit path loss  $1/L_g$  and distance  $y_1$  from the emitter to the ellipse center by axis length  $b$ , as shown in Table I.

### III. ANTENNA PERFORMANCE COMPARISON FOR AD-HOC NETWORK

#### A. Transmitter Configuration and Receiver Distribution

Consider the antenna array structure shown in Figure 5(a), where the black curve represents the antenna structure, and the red ellipse area represents the effective coverage of single antenna. The design of antenna array involves  $N$  directional antennas and elevation angle  $\alpha$  of each single antenna. The divergence angle of each antenna element is given by  $\phi_d = 360^\circ/N$ , and the coverage is related to the transmission power,  $N$  and  $\alpha$ . For comparison, an omnidirectional antenna is shown in Figure 5(b). The red circular area is the effective coverage of the antenna.

In order to compare the performance of different antennas structure, we assume an ad-hoc network and compare the performance of different antenna arrays. Assume that the node distribution in the network satisfies Poisson point process (PPP). For area  $S$ , the number of nodes  $M$  satisfies Poisson distribution with mean  $\lambda S$ , given by,

$$P(M = m) = \frac{(\lambda S)^m}{m!} e^{-(\lambda S)}, \quad (17)$$

where  $\lambda$  is the node intensity.

The path gain can be calculated directly based on the relative position of neighbor nodes. As shown in Figure 6, assuming pointing direction  $\gamma$  for a directional antenna of node  $A$  is known, and the neighbor node position  $B(x, y)$  can also be obtained through neighbor node estimation. The coordinates

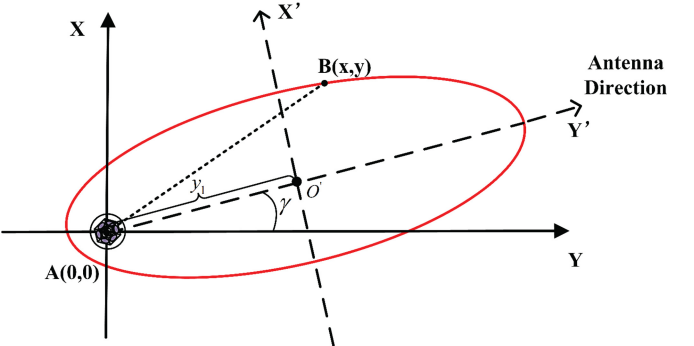


Fig. 6. The geometric model for the coverage area.

of  $B$  can be converted via rotation by Eq. (18), and then, according to the coverage intensity contour via an ellipse, we consider ellipse Eq. (19), where the major axis  $b$  of the ellipse can be calculated. The path loss can be calculated according to Table I. Equations (18) and (19) can be expressed as follows,

$$\begin{cases} x' = x \cos \gamma - y \sin \gamma; \\ y' = y \cos \gamma + x \sin \gamma - y_1; \end{cases} \quad (18)$$

$$\frac{x'^2}{a^2} + \frac{y'^2}{b^2} = 1, \quad (19)$$

where  $a = b \sin \alpha$  and  $y_1$  can be obtained from Table I, and based on the relative positions of  $A$  and  $B$ .

Next, letting  $\nu$  denote the optical frequency,  $P^r$  denote the receiving power of the receiver, and the arrival rate of signal photons, denoted as  $\Lambda$ , is given by

$$\Lambda = \frac{P^r \eta_f \eta_r}{h\nu}, \quad (20)$$

where  $\eta_f$  (typically 0.1) is the UV optical filter efficiency;  $\eta_r$  (typically 0.2) is the detector quantum efficiency; and  $h$  is the Planck's constant and the energy per photon is  $h\nu$ . Typically for an UV communication system,  $\nu$  is the frequency corresponding to wavelength of 266nm [14].

The maximum solar background radiation is approximately  $5 \times 10^4$  counts per second in the UV band [25]. Thus by calculation, setting the minimum receiving electric power of the receiver  $P_{\min}^r = 10^{-11} W$ , about 5 times larger than that of the background noise, the condition that node  $i$  ( $1 \leq i \leq m$ ) can communicate to node  $j$  ( $1 \leq j \leq m$ ) is given as follows,

$$P_i^t \cdot g_{i,j} \geq P_{\min}^r, \quad (21)$$

where  $P_i^t$  denotes the transmit power of node  $i$ ,  $g_{i,j}$  denotes the link gain from node  $i$  to node  $j$ . We aim to construct a graphs  $G = \langle V, E \rangle$ , where  $V = \{v_1, v_2, \dots, v_m\}$  denotes the node set and  $E = \begin{bmatrix} e_{1,1} & \cdots & e_{1,n} \\ \vdots & \ddots & \vdots \\ e_{n,1} & \cdots & e_{n,n} \end{bmatrix}$  denotes the edge set. For  $P^r \geq P_{\min}^r$ , we have  $e_{i,j} = 1$ ; otherwise  $e_{i,j} = 0$ .

#### B. System Analysis Model

In order to compare the performance of different antenna arrays, two performance metrics are analyzed, namely the probability of network connectivity and the power required for network connectivity.

1) *Network Connectivity Probability*: For any network, the network is connected if any two points can communicate through one or multiple hops. Defining  $C \triangleq E^{m-1}$ , the conditions for network connectivity are given by

$$c_{i,j} \neq 0, \forall i, j \in [1, m]. \quad (22)$$

2) *Power Required for Network Connectivity*: For edge  $e = (i, j) \in E$ , the transmission power on edge  $e$ , denoted as  $P_e$ , is given by

$$P_e = P_i^t + P_j^t. \quad (23)$$

We aim to obtain a tree with the minimum power on the edges. More specifically, we select  $m-1$  edges from edge set  $E$  to form a connected tree, denoted as  $T$  with mean power  $\frac{1}{m-1} \sum_{e \in T} P_e$ . The optimization problem can be expressed as follows,

$$\begin{aligned} \mathbf{P1:} \quad & \min_T \frac{1}{m-1} \sum_{e \in T} P_e \\ \text{s.t.} \quad & P_i^t \cdot g_{i,j} \geq P_{\min}^r; \\ & P_e = P_i^t + P_j^t; \\ & T \text{ forms a connected graph.} \end{aligned} \quad (24)$$

Based on the power threshold, we can obtain the minimum power on each link according to Eq. (21), and search the connected tree that minimizes the summation of the minimum power on the edges. **P1** is essentially the minimum spanning tree (MST) problem and can be solved by existing Prim algorithm, whose computational complexity grows linearly with the number of edges and thus in the square order with the number of nodes. Assuming node set  $V$ , randomly select a node from set  $V$  to initialize set  $U$ . Repeat the following process until set  $U$  contains  $m$  nodes. Choose edge  $(u, v)$  with the minimum power, where node  $u$  belongs to set  $U$  and node  $v$  belongs to set  $V - U$ , and add node  $v$  to set  $U$  with the power on edge  $P_e$ .

We outline the following scheme as the performance comparison benchmark. First, each node increases the transmission power for each antenna until the network becomes connected, and for directional antenna array, each antenna's power is  $1/N$  of the node power. Then, turn off the antennas that do not communicate, under the constraint that the network still keeps connected. The power sum corresponding to the MST topology is denoted as  $P_{\text{Dire}}^{\text{MST}}$ . For omnidirectional antenna structure, each node gradually reduces power to the critical value, under the constraint that the number of covered nodes is unchanged. The minimum power for MST topology is denoted as  $P_{\text{Omni}}^{\text{MST}}$ .

### C. Network Connectivity Probability

The network parameters are shown in Table II. Here,  $\alpha = 30^\circ$  is adopted for simulating the different numbers of antenna array  $N$ . Each node equally divides the power on all directions. Assuming node density  $\lambda = 40/\text{km}^2$ , Figure 7 shows a network randomly generated, where the network under the directional antenna array has more alternative paths, resulting in better MST performance.

TABLE II  
KEY PARAMETERS OF SIMULATION

Symbol	Physical meaning	Value/unit
$S$	Simulation area size	$1\text{ km}^2$
$N$	Number of directional antenna arrays	6
$\alpha$	Directional antenna elevation angle	$30^\circ$
$N_0$	Single case simulation times	20
$P_t$	Given power per node	$0.1\text{ W}$
$P_{\min}^r$	Minimum reception power threshold	$10^{-11}\text{ W}$

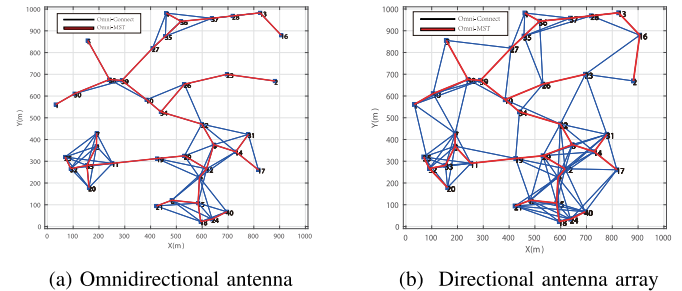


Fig. 7. The network obtained from the proposed approach with MST under different antennas.

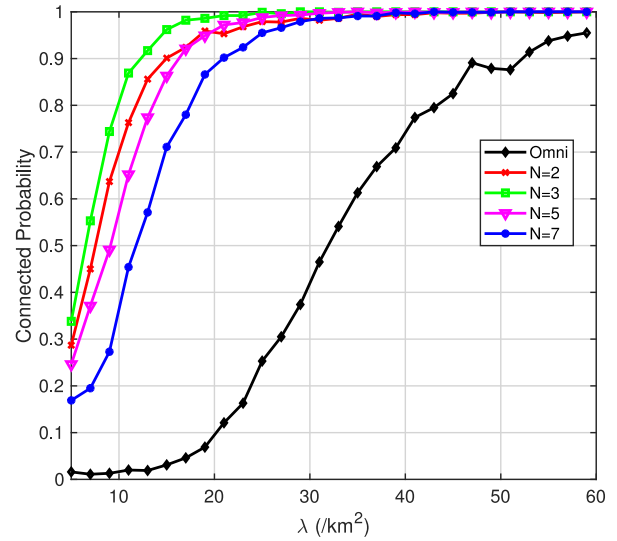


Fig. 8. Probability of connectivity under different antenna numbers.

We show the relationship between the number of antennas and the connection probability. According to the parameters in Table II, a network topology is randomly generated. With fixed parameters, 1000 node distribution realizations are randomly generated according to PPP distribution. The ratio of network being connected for different antenna numbers  $N$  is shown in Figure 8. It is observed that the nodes using the directional antenna array structure are easier to construct a connected network. Antenna number  $N = 3$  leads to the largest connection probability, but the connected probability is not sensitive to the number of antennas. In real communication, array sizes 2–7 are recommended according to the numerical results. Since the size of two antennas requires angle  $180^\circ$ , which is difficult to realize, typically array sizes 3 to 7 are recommended.

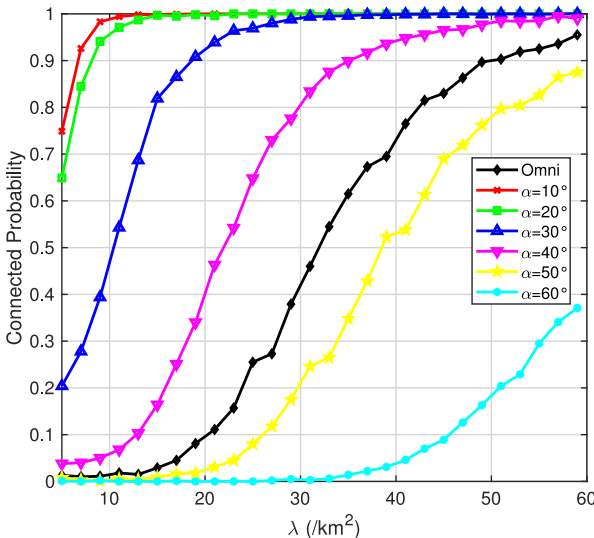


Fig. 9. Probability of connectivity at different antenna elevation angles.

We also investigate the connectivity probabilities at different elevation angles  $\alpha$ , as shown in Figure 9. It can be seen that lower elevation angle leads to higher connection probability. For elevation angle larger than  $40^\circ$ , the connectivity probability is lower than that of the omnidirectional antenna, so the recommended elevation angle lies between  $10^\circ$  and  $40^\circ$ .

#### D. Power Required for Network Connectivity

For simulation parameters shown in Table II, we compare the MST power required for network connectivity. For node density  $\lambda$  varying from 10 to 30 nodes per  $\text{km}^2$ , the power for different numbers of antennas is shown in Figure 10. Similarly, the power for different elevation angles is shown in Figure 11.

It can be seen from Figure 10 that the directional antenna array can effectively reduce the average transmission power, especially for low node intensity. This is because that more antennas result in more MST paths and thus lower power. Since the required power when  $N = 2$  is 1.5 times that when  $N = 3, 3\text{--}7$  is recommended for  $N$ . The effect of elevation angle of the array antenna on the MST power is similar to that of the connection probability. Lower elevation angle leads to lower power for connectivity. The required power when  $\alpha = 60^\circ$  and  $\alpha = 50^\circ$  is 1.5 times more than  $\alpha = 40^\circ, 10^\circ\text{--}40^\circ$  is recommended for  $\alpha$ .

According to the numerical results, feasible number of antennas can be selected between 3 and 7, and larger  $N$  can provide greater space division gain, but increasing the number of antennas will increase the realization complexity. Higher elevation angle increases the probability of link blockage, the range of elevation angle can be selected between  $20^\circ$  and  $40^\circ$ .

## IV. POWER ALLOCATION FOR TWO-LAYER UV COMMUNICATION NETWORK

### A. Two-Layer Network Model

We consider a two-layer network, where each first-layer node adopts the directional array antenna as the transmitter, and each second-layer node adopts an omnidirectional antenna

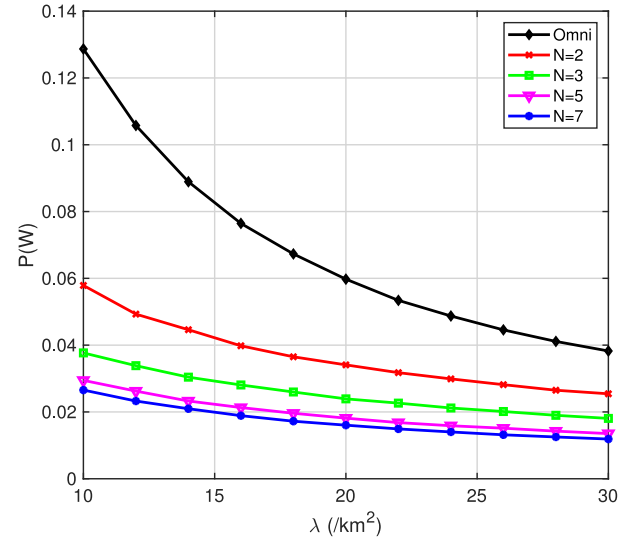


Fig. 10. The MST power under different antenna numbers.

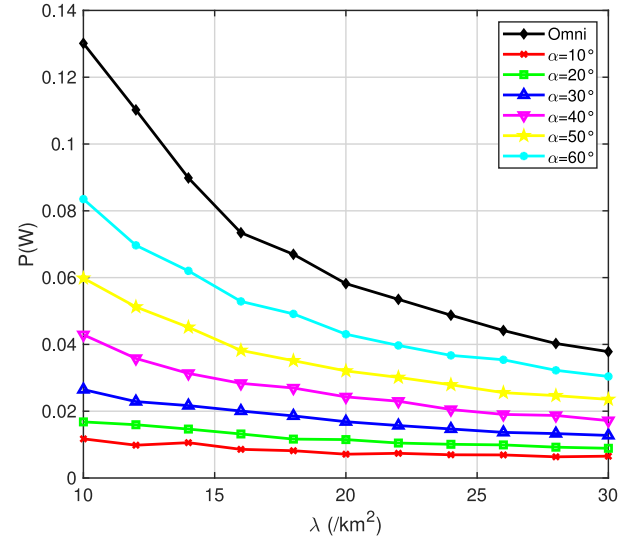


Fig. 11. The MST power under different elevation angles.

structure as a receiver, as shown in Figure 12. According to feasible values on the number of antennas and elevation angle in the last paragraph of Section III, the number of antennas is set as  $N = 6$ , and the elevation angle  $\alpha$  is set as  $30^\circ$ .

The distribution of nodes satisfies uniform poisson point distribution, with densities  $\lambda_1$  and  $\lambda_2$  for the first-layer and second-layer nodes, respectively, with ratio  $k = \frac{\lambda_2}{\lambda_1}$ . The second-layer node is expected to be accessible within the ellipse range of the first-layer node, and the corresponding power of the receiving intensity contour line is  $P_{\min}^r$ .

### B. Interference Optimization Problem

For a two-layer network, assume that there are  $M_1$  first-layer nodes and  $M_2$  second-layer nodes, and that each first-layer node has  $N$  antennas, where antenna  $i$  belongs to the first-layer node  $[i/N]$ . Let  $\mathbf{P}^t = (P_1^t, P_2^t, \dots, P_{M_1N}^t)$  denote the power of transmission antennas, and  $\mathbf{P}^r =$

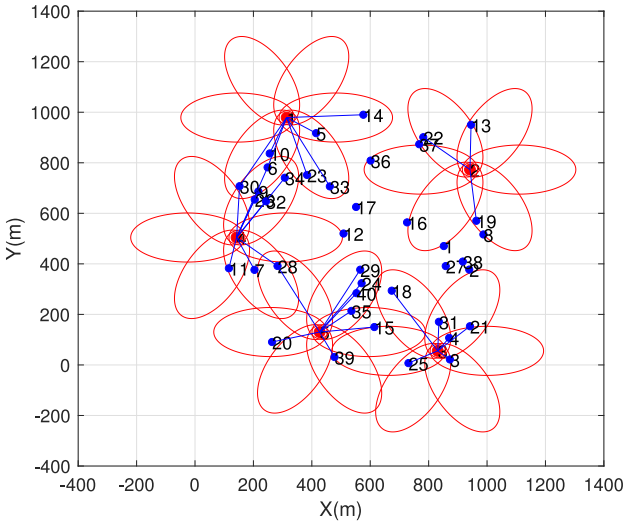


Fig. 12. The converge illustration of the two-layer UV ad-hoc network.

$(P_1^r, P_2^r, \dots, P_{M_2}^r)$  denote the received power of the second-layer. Then, we have

$$\mathbf{P}^r = \mathbf{P}^t \cdot \mathbf{G} + n \quad (25)$$

where  $\mathbf{G} \triangleq \begin{bmatrix} g_{1,1} & \cdots & g_{1,M_2} \\ \vdots & \ddots & \vdots \\ g_{M_1 N, 1} & \cdots & g_{M_1 N, M_2} \end{bmatrix}$  denotes the non-line-

of-sight path gain derived according to Table I, and  $n$  denotes the power of background radiation with arrival rate  $5 \times 10^4$  counts per second in the UV band [25]. According to Eq. (20), the power of transmitting antenna of the first-layer node can be calculated.

Each second-layer node selects the antenna of the first-layer node with the highest signal intensity for access. Assume minimum receiving power  $P_{\min}^r$  to determine whether the second-layer node can be accessed, and each node only selects at most one antenna to access. Define access matrix as follows,

$$\mathbf{A} = \begin{bmatrix} a_{1,1} & \cdots & a_{1,M_2} \\ \vdots & \ddots & \vdots \\ a_{M_1 N, 1} & \cdots & a_{M_1 N, M_2} \end{bmatrix}. \quad (26)$$

For any second-layer node  $j$  and antenna  $i$ ,  $a_{i,j}$  is given as

$$\begin{cases} a_{i,j} = 1, & P_{i,j}^r \geq P_{\min}^r \text{ and } P_{i,j}^r = \max_i(P_{i,j}^r), \\ & i \in [1, M_1 N]; \\ a_{i,j} = 0, & P_{i,j}^r < P_{\min}^r \text{ or } P_{i,j}^r < \max_i(P_{i,j}^r), \\ & i \in [1, M_1 N]; \end{cases} \quad (27)$$

where  $P_{i,j}$  denotes the received power of the second-layer node  $j$  from antenna  $i$ .

We evaluate the network capacity based on that of a continuous-time poisson channel, assuming mean numbers  $\chi$  for the signal and  $\beta$  of background radiation photons, respectively. Define the signal-to-noise ratio as  $s = \frac{\chi}{\beta}$ . According to [26]–[28], the optimal duty cycle, denoted as  $\mu^*$ , is given

by [27]

$$\mu^* = \left( \frac{\left(1 + \frac{\chi}{\beta}\right)^{(1+\beta)}}{e} - 1 \right) \frac{\beta}{\chi} = \left( \frac{(1+s)^{(1+\frac{1}{s})}}{e} - 1 \right) \frac{1}{s}; \quad (28)$$

where the background interference of ultraviolet scattering communication is stable. At the same time, the second-layer nodes will transmit information with a fixed power, such that the first-layer nodes can get the perfect CSI and set the optimal power.

The capacity, denoted as  $C$ , is given by Equations (29). It is seen that given signal intensity  $\chi$  the capacity decreases with interference intensity  $\beta$ ; given interference intensity  $\beta$  the capacity increases with signal intensity  $\chi$ ; and given signal intensity  $\chi$  the capacity increase with  $s$ .

$$\begin{aligned} C = & -\chi \left( \mu^* + \frac{1}{s} \right) \ln \left( \mu^* + \frac{1}{s} \right) \\ & + \mu^* \chi \left( 1 + \frac{1}{s} \right) \ln \left( 1 + \frac{1}{s} \right) + (1 - \mu^*) \frac{\chi}{s} \ln \frac{1}{s}. \end{aligned} \quad (29)$$

In this work, we assume that perfect CSI is available at the first-layer nodes. This can be justified by the fact that the background radiation intensity can be estimated accurately, and the long coherent time of UV NLOS channel leads to accurate channel estimation.

In order to calculate the capacity, we need to obtain the signal intensity and interference of each second-layer node. Let  $I_j$  and  $N_j$  denote the signal intensity and interference intensity at second-layer node  $j$ , respectively, which can be calculated as follows,

$$I_j = \sum_{i=1}^{M_1 N} P_{i,j}^r \cdot a_{i,j} \frac{\eta_f \eta_r}{h\nu}, \quad j \in [1, M_2], \quad (30)$$

$$N_j = \sum_{i=1}^{M_1 N} P_{i,j}^r \frac{\eta_f \eta_r}{h\nu} - I_j, \quad j \in [1, M_2]. \quad (31)$$

The Signal-to-Interference-Plus-Noise Ratio (SINR) can be given as follows,

$$\text{SINR}_i = \frac{\sum_{i=1}^{M_1 N} P_{i,j}^r \cdot a_{i,j} \frac{\eta_f \eta_r}{h\nu}}{\sum_{i=1}^{M_1 N} P_{i,j}^r \frac{\eta_f \eta_r}{h\nu} + n}, \quad 1 \leq i \leq M_1 N. \quad (32)$$

We consider the following constraints.

**Peak Power Constraint:** The transmission power  $P_i$  on each antenna  $i$  for the first-layer nodes cannot exceed the maximum one, given by  $P_{\max}^t$ , i.e.,

$$P_i \leq P_{\max}^t, \quad 1 \leq i \leq M_1 N. \quad (33)$$

**Second-layer Node Access Constraint:** It is easily seen that according to indicators  $\{a_{i,j}\}_{1 \leq i \leq M_1 N, 1 \leq j \leq M_2}$ , the maximum number of second-layer nodes can be accessed. After the power allocation, letting  $a'_{i,j}$  indicate whether node  $i$  can access transmission antenna  $j$ , the number of second-layer

nodes that can be accessed does not change, i.e.,

$$\sum_{i=1}^{M_1 N} \sum_{j=1}^{M_2} a_{i,j} = \sum_{i=1}^{M_1 N} \sum_{j=1}^{M_2} a'_{i,j}. \quad (34)$$

**Interference Constraint:** Each second-layer node sets a lower bound on the SINR, i.e.,

$$SINR_j \geq SINR_{th}, \quad 1 \leq j \leq M_2. \quad (35)$$

We aim to maximize the minimum non-zero transmission rate. More specifically, for rate  $C_j$  for second-layer node  $j$ , define the minimum positive rate as  $C_{min} = \min_{1 \leq j \leq M_2, C_j > 0} (C_j)$ .

Consider optimizing the worst node performance without sacrificing overall performance too much. Then, we construct a constraint that the sum capacity is larger than or equal to  $\gamma$  times of the initial sum capacity, obtained from  $\{a_{i,j}\}_{1 \leq i \leq M_1 N, 1 \leq j \leq M_2}$ , i.e.,  $\sum_{j=1}^{M_2} C_j \geq \gamma C_0$ , where  $C_0$  is the sum capacity when all the antenna power is set to the maximum power.

Thus, the problem can be formulated as follows,

$$\begin{aligned} \mathbf{P2:} \quad & \max_{\{P_i\}_{i=1}^{M_1 N}} C_{min} \\ \text{s.t.} \quad & P_i \leq P_{max}^t, \quad 1 \leq i \leq M_1 N; \\ & \sum_{j=1}^{M_2} C_j \geq \gamma C_0; \\ & \sum_{i=1}^{M_1 N} \sum_{j=1}^{M_2} a_{i,j} = \sum_{i=1}^{M_1 N} \sum_{j=1}^{M_2} a'_{i,j} \\ & SINR_j \geq SINR_{th}, \quad 1 \leq j \leq M_2. \end{aligned} \quad (36)$$

### C. A Heuristic Solution to Transmission Power Optimization

We propose the heuristic approach to solve Problem **P2**, including node allocation via Algorithm 1, and power allocation via Algorithm 2.

First, we set the antenna power of the first-layer nodes to the maximum power  $P_{max}^t$ , determine the antennas that can be covered, and allocate the nodes to the antennas evenly, to ensure that the nodes can preempt the channel fairly, where the node allocation matrix is denoted as  $D$ . Then, according to matrix  $D$ , we calculate the SINR of each second-layer node, select a part of the second-layer nodes with the lowest SINR to construct an optimized target node set  $S$ , and iteratively adjust the power of antenna  $Q$  corresponding to node set  $S$ , to optimize performance of the worst node.

### D. Numerical and Simulation Results

Considering the similarities between the proposed network and cell-free network, we adopt a typical power allocation algorithm which is called “SINR Ranking Power Allocation” for comparison [29]. Compared with the original method in [29], in order to better solve **P2**, the algorithm is modified, using SINR as the ranking index, and the power is allocated hierarchically. In the benchmark approach, the power is equally divided according to the number of accessible nodes.

---

### Algorithm 1 Node Allocation Algorithm

- 1: **Input:** Second-layer node position  $(x, y)$ , transmitter elevation angle  $\alpha$ , number of transmission antenna  $N$ , direction of antenna  $\gamma$ , initialization parameters  $A, B, C$ .
  - 2: Calculate axis length  $b$  from  $(x, y)$  (18) and (19);
  - 3: Bring the  $\alpha$  and  $b$  into Table II to get path loss  $L_g$  between first-layer node and second-layer node;
  - 4: Calculate the received power of each second-layer node based on  $L_g$  and  $P_{max}^t$ ;
  - 5: The second-layer node selects the antenna corresponding to the maximum received power to access according to Equation (27), and obtains matrix  $A$ .
  - 6: Turn off the antenna that does not cover the second-layer node .
  - 7: **Perform node allocation:**
  - 8: **for**  $j = 1 : M_2$
  - 9:   **if** Node covered by multiple antennas
  - 10:     The second-layer node is assigned to the antenna with the least coverage node;
  - 11:   **if** The minimum number of nodes covered by the corresponding antenna is equal
  - 12:     Assign to the antenna with smaller path loss  $L_g$ ;
  - 13:   **end if**
  - 14: **end if**
  - 15: **end for**
  - 16: Construct allocation matrix  $D$ , where  $d_{i,j} = 1$  indicates that second-layer node  $j$  is assigned to transmitting antenna  $i$ .
  - 17: **Output:** The second-layer node allocation matrix  $D$ ;
- 

### Algorithm 2 Iteratively Power Allocation Algorithm

- 1: **Input:** Node allocation matrix  $D$ , Link loss matrix  $L$ , initialization parameters  $\zeta, \xi$ .
  - 2: **while** Constraints are not met *or* Minimum rate no longer increases **do**
  - 3:   Update link gain matrix  $g'_{i,j} = g_{i,j} d_{i,j}$ , recalculate SINR according to the formula (35) and sort in reverse order;
  - 4:   Select the second-layer node corresponding to the lowest SINR ratio of  $\zeta$  to form set  $S$ , for example  $\zeta = 20\%$ ;
  - 5:   Find the corresponding antenna set  $Q$ ;
  - 6:   Find the antenna that interferes with  $S$  in complement  $M_2 - Q$ , and reduce the power by  $\xi$ ;
  - 7:   Update power matrix  $P^t$ ;
  - 8:   Calculate capacity index according to the formula (29);
  - 9: **end while**
  - 10: **Output:** Capacity sum  $\sum_{j=1}^{M_2} C_j$  and the minimum capacity  $C_{min}$ ;
- 

The SINRs are sorted in the ascending order, from small to large, and the power is sorted in the descending order, which generates an one-to-one correspondence. The maximum power is assigned to the node with minimum SINR.

TABLE III  
KEY PARAMETERS OF SIMULATION

Symbol	Physical meaning	Value/unit
$S$	Simulation area size	$2\text{km}^2$
$N_0$	Single case simulation times	100
$SINR$	Signal to interference plus noise ratio	3dB
$\psi$	Sum capacity constraint ratio	80%
$\zeta$	Minimum capacity set ratio of selected nodes	20%
$\xi$	Ratio of each power down	20%

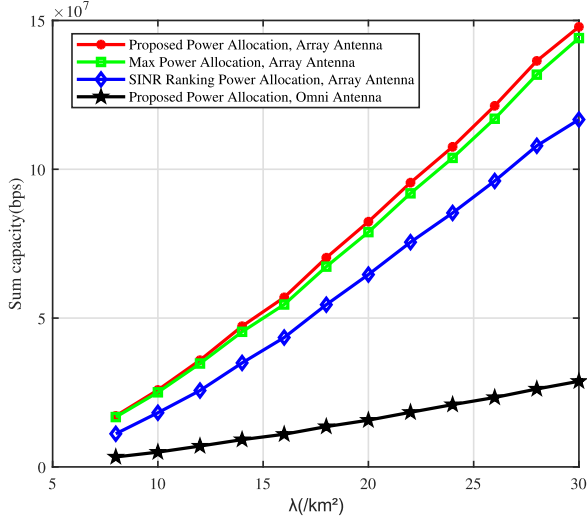


Fig. 13. The sum capacity of the second-layer nodes at different first-layer node densities.

We compare the sum and minimum rates of the second-layer nodes of the proposed “Max Power Allocation” under different antenna structures, “SINR Ranking Power Allocation” and “Proposed Power Allocation”. The main simulation parameters are shown in Table III, while others the same as those in Table I, assuming node ratio  $k = 20$ .

The sum and minimum user capacities with respect to the first-layer node density are shown in Figure 13 and Figure 14, respectively. It can be seen from Figure 14 that the “Proposed Power Allocation” algorithm has higher sum capacity compared with “SINR Ranking Power Allocation” and “Max Power Allocation”. The comparison between omnidirectional antenna and directional array antennas using the same “Proposed Power Allocation” algorithm also demonstrates the advantages of array antennas. It also can be seen that the “Proposed Power Allocation” algorithm has higher minimum rate than “Max Power Allocation” with approximately the gain of 10%–20%, and approximately the same as “SINR Ranking Power Allocation” for node density  $\lambda > 12$ .

The convergence of the proposed algorithm is tested under several typical node density  $\lambda$ , as shown in Figure 15. It can be found that larger node density  $\lambda$  leads to slower convergence, for example, for  $\lambda = 20$ , 18 iterations are needed for convergence.

We also simulated the impact of different node ratios  $k$  on the two indicators, assuming node density  $\lambda = 20$ . The results are shown in Figures 16 and 17, and the convergence of the

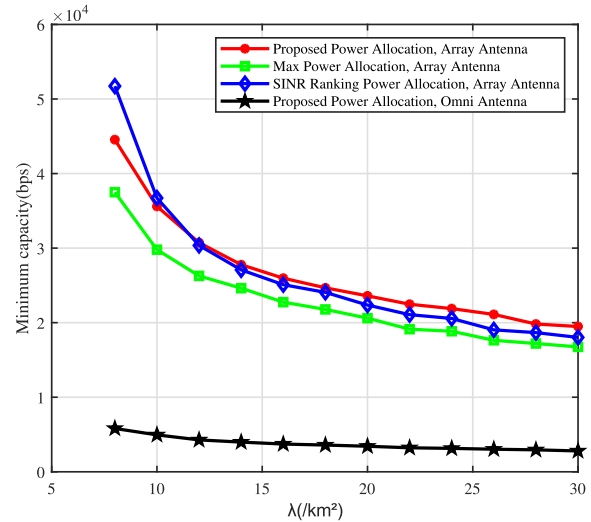


Fig. 14. The minimum capacity of the second-layer nodes at different first-layer node densities.

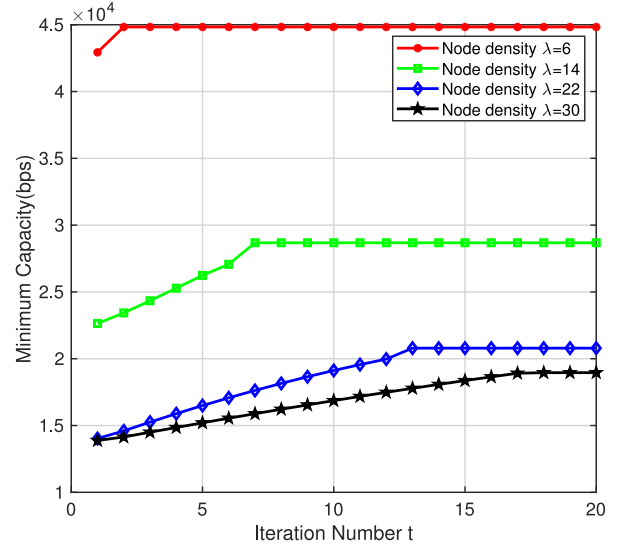


Fig. 15. Convergence of the algorithm under different node densities.

algorithm under different node ratios  $k$  is shown in Figure 18. It can be seen that the results are basically of the same trend as those of different node densities. Larger ratio  $k$  leads to slower convergence.

#### E. Simulation Results of Joining the MAC Protocol

In order to verify the performance gain of the proposed power allocation with overhead of a MAC layer protocol, we adopt CMSA/CA-based protocol. If multiple second-layer nodes access the same antenna at the same time, they compete the downlink channel by requesting. The MAC layer protocol simulation parameters are shown in Table IV [30].

With MAC layer protocol, the sum and minimum throughputs are shown in Figure 19 and Figure 20, respectively. It is shown that with the competition protocol, the rate of the worst node is still comparable to that of algorithm “SINR Ranking Power Allocation”, due to small difference

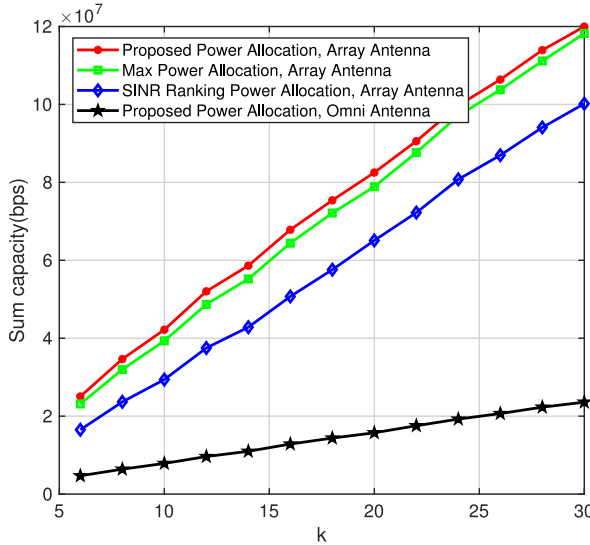


Fig. 16. The sum capacity of algorithm performance under different node ratio  $k$ .

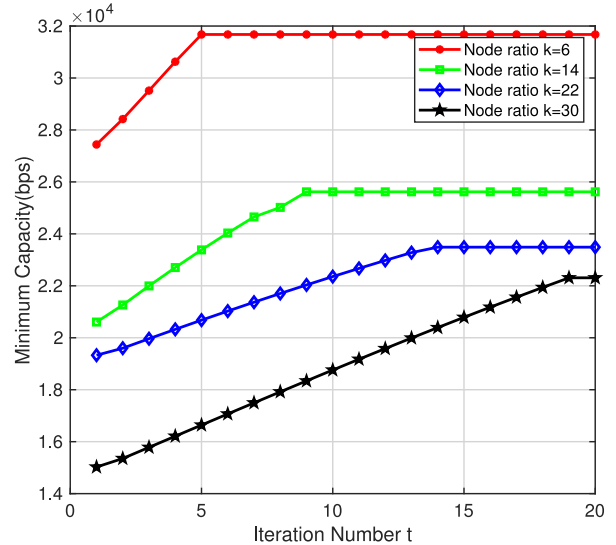


Fig. 18. Convergence of the algorithm under different node ratio  $k$ .

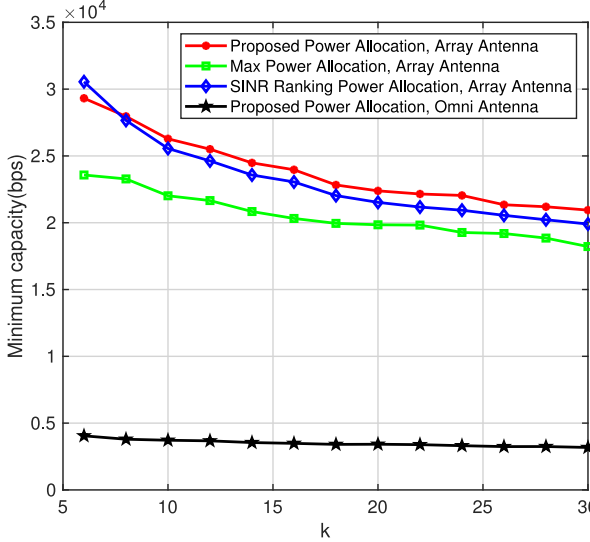


Fig. 17. The minimum capacity of the second-layer nodes at different node ratios  $k$ .

TABLE IV  
KEY PARAMETERS OF SIMULATION

Physical meaning	Value/unit
SIFS	10 $\mu$ s
DIFS	50 $\mu$ s
Slot time	20 $\mu$ s
Node random request rate	50
Request packet length	2.5ms
TotalTimeInSeconds	20s

in the node capacity and the randomness of competing access. But the improvement over the “Max Power Allocation” still remains. At the same time, the sum rate still higher than that of “SINR Ranking Power Allocation” and “Max Power Allocation”. Using omni-directional antenna degrades the sum rate, since a single transmission node serves multiple nodes with lower link gain. We also simulated the impact of adding

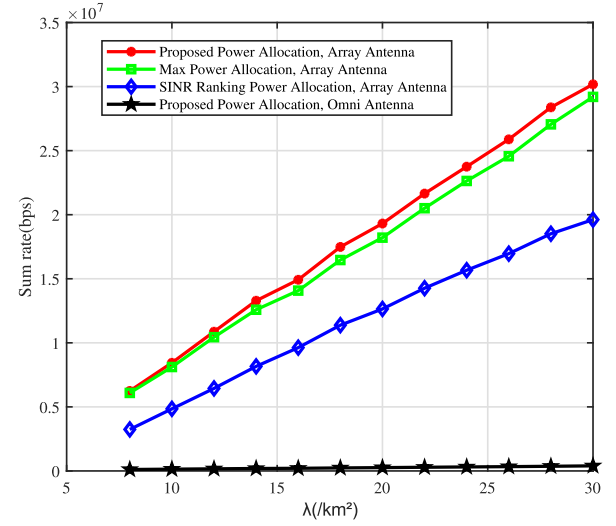


Fig. 19. The sum rate of the second-layer nodes at different first-layer node densities.

the MAC layer protocol under different node ratios  $k$ , and the results are basically the same as the density of different nodes  $\lambda$ .

The adopted MAC layer protocol is the CSMA/CA in 802.11, where the same channel is shared by multiple second-layer nodes covered by the same antenna. Due to random channel preemption, the effective rate and relative capacity will be reduced, and the throughput difference between different algorithms will be reduced. Since the first-layer nodes equipped with omnidirectional antennas need to serve more second-layer nodes at the same time with lower link gain, the throughput of a single second-layer node will degrade.

#### F. Performance Under Link Gain Estimation Errors

Recall that to evaluate the link gains, it is necessary to estimate the position of the secondary-order nodes from the first-order nodes [24]. Since there exists estimation errors

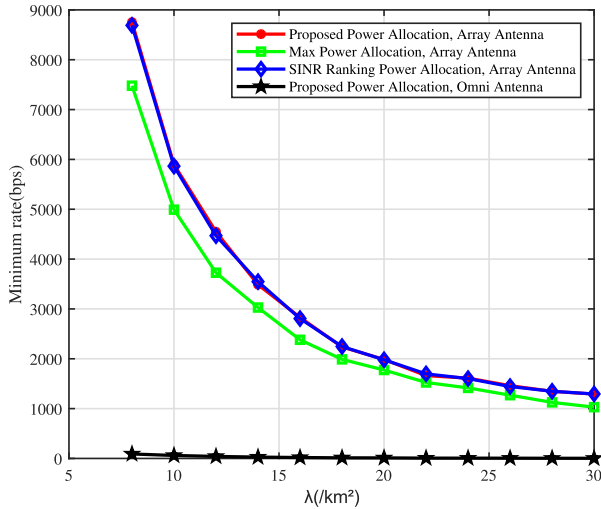


Fig. 20. The minimum rate of the second-layer nodes at different first-layer node densities.

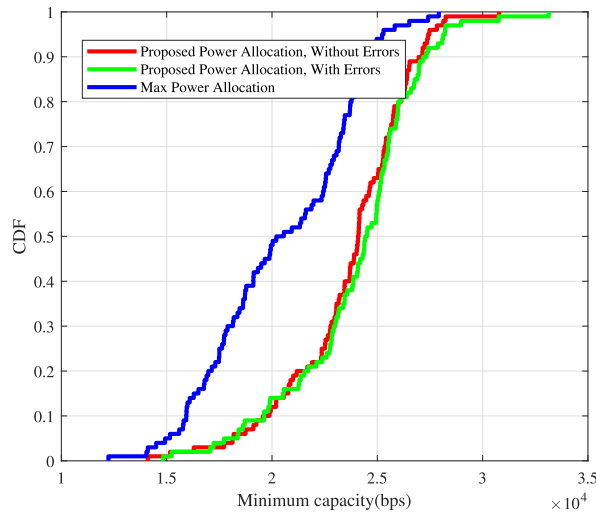


Fig. 21. CDF of the minimum capacity with or without error.

inevitably, it is necessary to investigate the robustness of the proposed approach under estimation error.

Assume that for actual position  $(\theta, r)$ , the angle and radius estimates are given as follows,

$$\begin{cases} \theta_{err} = \theta + \Delta\theta, \\ r_{err} = r + \Delta r, \end{cases} \quad (37)$$

where  $\Delta\theta$  and  $\Delta r$  are angle and distance estimation errors, respectively.

We set the maximum estimated distance estimate error to be 20m and the maximum angle to be  $10^\circ$ , and  $\Delta r \in [-20, 20]m$ ,  $\Delta\theta \in [-10^\circ, 10^\circ]$ , both satisfying uniform distribution. According to the link gains from the position estimate, the network adopts the proposed algorithm to obtain the power of each antenna. For the first-layer node density 20, we conduct multiple random simulations and obtain the CDF of minimum capacity with CSMA protocol, as shown in Figure 21, and the CDF of minimum rate shown in Figure 22, respectively. It is seen that the proposed method shows robustness to the estimation error, and the rate of “Proposed Power

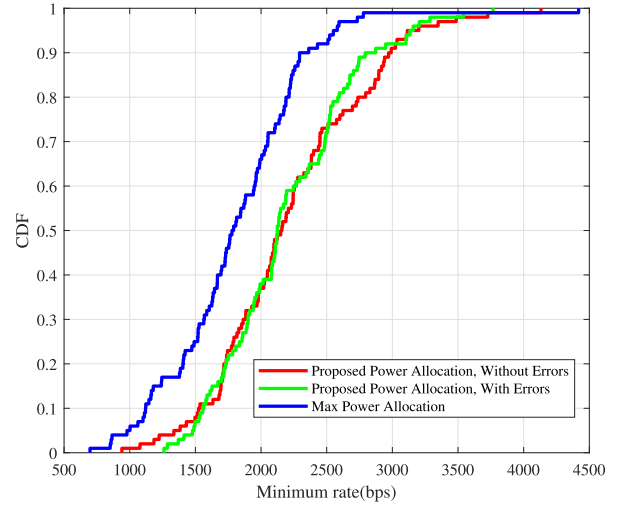


Fig. 22. CDF of the minimum rate with or without error.

Allocation” is still higher than that of “Max Power Allocation” after adding MAC protocol.

## V. CONCLUSION

We have characterized the link gain of NLOS UV scattering communication, which shows that the coverage contour is approximately elliptical. The connectivity and minimum power of different antenna structures in the UV scattering network are compared. Numerical results show that directional antenna array has higher access probability and lower connected power than omnidirectional antenna, and give the recommended optimal antenna structure design parameters. In addition, we consider the layered ultraviolet scattering network and propose a power allocation algorithm to reduce the interference. It can be seen that the directional antenna arrays perform better than the omnidirectional antenna when adopted by first-layer node, and the proposed power allocation scheme can improve the rate of the worst node by more than 10% compared with the approach for cell-free network based on SINR ranking.

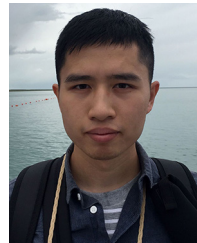
## REFERENCES

- [1] H. Qi, D. Zou, C. Gong, and Z. Xu, “Two-dimensional intensity distribution and connectivity in ultraviolet ad-hoc network,” in *Proc. IEEE Int. Conf. Commun. (ICC)*, Dublin, Ireland, Jul. 2020, pp. 1–6.
- [2] Z. Xu and B. M. Sadler, “Ultraviolet communications: Potential and state-of-the-art,” *IEEE Commun. Mag.*, vol. 46, no. 5, pp. 67–73, May 2008.
- [3] H. Ding, G. Chen, A. K. Majumdar, B. M. Sadler, and Z. Xu, “Modeling of non-line-of-sight ultraviolet scattering channels for communication,” *IEEE J. Sel. Areas Commun.*, vol. 27, no. 9, pp. 1535–1544, Dec. 2009.
- [4] R. M. Gagliardi and S. Karp, *Optical Communications*, 2nd ed. New York, NY, USA: Wiley, 1995.
- [5] R. Drost, T. Moore, and B. Sadler, “Ultraviolet scattering propagation modeling: Analysis of path loss versus range,” *J. Opt. Soc. Amer. A, Phot. Image Sci. Vis.*, vol. 30, no. 11, pp. 2259–2265, Nov. 2013.
- [6] G. Chen, L. Liao, Z. Li, R. J. Drost, and B. M. Sadler, “Experimental and simulated evaluation of long distance NLOS UV communication,” in *Proc. 9th Int. Symp. Commun. Syst. Netw. Digit. Signal Process. (CNSDSP)*, Manchester, U.K., Jul. 2014, pp. 904–909.
- [7] Q. He, Z. Xu, and B. M. Sadler, “Performance of short-range non-line-of-sight LED-based ultraviolet communication receivers,” *Opt. Exp.*, vol. 18, no. 12, pp. 12226–12238, Jun. 2010.

- [8] R. J. Drost, B. M. Sadler, and G. Chen, "Dead time effects in non-line-of-sight ultraviolet communications," *Opt. Exp.*, vol. 23, no. 12, pp. 15748–15761, Jun. 2015.
- [9] A. Gupta, M. Noshad, and M. Brandt-Pearce, "NLOS UV channel modeling using numerical integration and an approximate closed-form path loss model," in *Proc. SPIE Laser Commun. Propag. Atmosph. Oceans*, vol. 8517. San Diego, CA, USA, Aug. 2012, Art. no. 851709.
- [10] L. Wang, Y. Li, and Z. Xu, "On connectivity of wireless ultraviolet networks," *J. Opt. Soc. Amer. A*, vol. 28, no. 10, pp. 1970–1978, Oct. 2011.
- [11] A. Vavoulas, H. G. Sandalidis, and D. Varoutas, "Connectivity issues for ultraviolet UV-C networks," *IEEE/OSA J. Opt. Commun. Netw.*, vol. 3, no. 3, pp. 199–205, Mar. 2011.
- [12] D. Jin, T. Zhao, R. Xue, and L. Liu, "Analyzing of ultraviolet single scattering coverage for non-line-of-sight communication," in *Proc. 25th IET Irish Signals Syst. Conf. China-Ireland Int. Conf. Inf. Commun. Technol. (ISSC/CICT)*, Limerick, Ireland, Sep. 2014, pp. 316–321.
- [13] C. Xu, H. Zhang, and J. Cheng, "Effects of haze particles and fog droplets on NLOS ultraviolet communication channels," *Opt. Exp.*, vol. 23, no. 18, pp. 23259–23269, Sep. 2015.
- [14] Z. Xu, H. Ding, B. M. Sadler, and G. Chen, "Analytical performance study of solar blind non-line-of-sight ultraviolet short-range communication links," *Opt. Lett.*, vol. 33, no. 16, pp. 1860–1862, Aug. 2008.
- [15] L. Wang, Z. Xu, and B. M. Sadler, "Non-line-of-sight ultraviolet link loss in noncoplanar geometry," *Opt. Lett.*, vol. 35, no. 8, pp. 1263–1265, Aug. 2010.
- [16] Y. Zuo, H. Xiao, J. Wu, W. Li, and J. Lin, "Closed-form path loss model of non-line-of-sight ultraviolet single-scatter propagation," *Opt. Lett.*, vol. 38, no. 12, pp. 2116–2118, Jun. 2013.
- [17] Y. Sun and Y. Zhan, "Closed-form impulse response model of non-line-of-sight single-scatter propagation," *J. Opt. Soc. Amer. A*, vol. 33, no. 4, pp. 752–757, Apr. 2016.
- [18] L. Liao, Z. Li, T. Lang, and G. Chen, "UV LED array based NLOS UV turbulence channel modeling and experimental verification," *Opt. Exp.*, vol. 23, no. 17, pp. 21825–21835, Aug. 2015.
- [19] N. Raptis, E. Pikasis, and D. Syvridis, "Power losses in diffuse ultraviolet optical communications channels," *Opt. Lett.*, vol. 41, no. 18, pp. 4421–4424, Sep. 2016.
- [20] Y. Li, L. Wang, Z. Xu, and S. V. Krishnamurthy, "Neighbor discovery for ultraviolet ad hoc networks," *IEEE J. Sel. Areas Commun.*, vol. 29, no. 10, pp. 2002–2011, Dec. 2011.
- [21] D. Kedar and S. Arnon, "Non-line-of-sight optical wireless sensor network operating in multiscattering channel," *Appl. Opt.*, vol. 45, no. 33, pp. 8454–8461, Nov. 2006.
- [22] A. Vavoulas, H. Sandalidis and D. Varoutas, "Node isolation probability for serial ultraviolet UV-C multi-hop networks," *IEEE/OSA J. Opt. Commun. Netw.*, vol. 3, no. 9, pp. 750–757, Sep. 2011.
- [23] D. M. Junge, "Non-line-of-sight electro-optic laser communications in the middle ultraviolet," Ph.D. dissertation, Naval Postgraduate School, Monterey, CA, USA, 1977.
- [24] H. Qi, C. Gong, and Z. Xu, "Omnidirectional antenna array-based transmitter direction sensing in ultra-violet ad-hoc scattering communication networks," in *Proc. IEEE Int. Conf. Commun. Workshops (ICC Workshops)*, Shanghai, China, Jul. 2019, pp. 1–6.
- [25] G. Wang, K. Wang, C. Gong, D. Zou, Z. Jiang, and Z. Xu, "A 1Mbps real-time NLOS UV scattering communication system with receiver diversity over 1km," *IEEE Photon. J.*, vol. 10, no. 2, pp. 1–13, Apr. 2018.
- [26] A. D. Wyner, "Capacity and error exponent for the direct detection photon channel. II," *IEEE Trans. Inf. Theory*, vol. 34, no. 6, pp. 1449–1471, Nov. 1988.
- [27] K. Chakraborty and P. Narayan, "The Poisson fading channel," *IEEE Trans. Inf. Theory*, vol. 53, no. 7, pp. 2349–2364, Jul. 2007.
- [28] M. R. Frey, "Information capacity of the Poisson channel," *IEEE Trans. Inf. Theory*, vol. 37, no. 2, pp. 244–256, Mar. 1991.
- [29] J. Beysens, Q. Wang, A. Galisteo, D. Giustiniano, and S. Pollin, "A cell-free networking system with visible light," *IEEE/ACM Trans. Netw.*, vol. 28, no. 2, pp. 461–476, Apr. 2020.
- [30] ISO/IEC 8802-11: 1999 *Information Technology—Telecommunications and Information Exchange Between Systems— Local and Metropolitan Area Networks—Specific Requirements—Part 11: Wireless LAN Medium Access Control (MAC) and Physical Layer (PHY) Specifications*, IEEE Standard Std 802.11, 2005.



**Hong Qi** received the B.S. degree in electrical engineering from Southwest Jiaotong University in 2018, and the M.S. degree in electrical engineering from the University of Science and Technology of China in 2021.



**Difan Zou** received the B.S. degree in applied physics and the M.S. degree in electrical engineering and information science from the University of Science and Technology of China in 2014 and 2017, respectively. He is currently pursuing the Ph.D. degree with the University of California at Los Angeles, Los Angeles, USA. His research interests rely on machine learning, optimization, wireless communication, and signal processing.



**Chen Gong** (Senior Member, IEEE) received the B.S. degree (minor) in electrical engineering and mathematics from Shanghai Jiaotong University, Shanghai, China, in 2005, the M.S. degree in electrical engineering from Tsinghua University, Beijing, China, in 2008, and the Ph.D. degree from Columbia University, New York, NY, USA, in 2012. He was a Senior Systems Engineer with Qualcomm Research, San Diego, CA, USA, from 2012 to 2013. He is currently a Faculty Member with the University of Science and Technology of China. His research interests include wireless communications, optical wireless communications, and signal processing. He received the Hongkong Qiushi Outstanding Young Researcher Award in 2016.



**Zhengyuan Xu** (Senior Member, IEEE) received the B.S. and M.S. degrees from Tsinghua University, China, and the Ph.D. degree from the Stevens Institute of Technology, USA. He was a tenured Full Professor with University of California at Riverside, Riverside, and later with Tsinghua University, before he joined the University of Science and Technology of China. He was the Founding Director of the Multi-Campus Center for Ubiquitous Communication by Light, University of California, and the Founding Director of the Wireless-Optical Communications Key Laboratory, Chinese Academy of Sciences. He was a Distinguished Expert and a Chief Scientist of the National Key Basic Research Program of China. He has published over 300 international journal and conference papers, and coauthored a book titled *Visible Light Communications: Modulation and Signal Processing* (Wiley-IEEE Press). He has been on the (Elsevier) annual list of Most Cited Chinese Researcher since 2014, and his works have received over 5000 citations according to Google Scholar. His research focuses on optical wireless communications, mobile networking, artificial intelligence, wireless big data, sensing, ranging, and localization. He has served as an associate editor for different IEEE/OSA journals and was a Founding Chair of IEEE Workshop on Optical Wireless Communications in 2010.